Available online at www.sciencedirect.com
SCIENCE DIRECT®
Journal of the European Ceramic Society 25 (2005) 1095–1107
www.elsevier.com/locate/jeurceramsoc

The thermally induced transformation of pseudoboehmite gels—a comparison of the effects of corundum seeding and iron doping

M. Nofz [a,*], R. Stösser [b], G. Scholz [b], I. Dörfel [a], D. Schultze [a]

[a] *Federal Institute for Materials Research and Testing, 12200 Berlin, Germany*
[b] *Institute of Chemistry, Humboldt-University, 12489 Berlin, Germany*

Received 24 January 2004; received in revised form 1 April 2004; accepted 20 April 2004
Available online 13 July 2004

Abstract

The transformation of doped or seeded pseudoboehmite to corundum was studied by combining thermal analysis, X-ray diffraction, transmission electron microscopy, and electron paramagnetic resonance spectroscopy. The temperature of phase transformation to corundum was lowered by about 130 °C when Fe^{3+} or corundum seeds were added to the sols. Action of Fe^{3+} ions depends on the actual degree of thermally induced transformation of pseudoboehmite via transition aluminas to corundum and the ability of these alumina phases to incorporate Fe^{3+} ions. These ions tend to aggregate with increasing iron concentration of the alumina phases and can work as nucleation centers. Small (∼20 nm) corundum particles act as active nucleation sites whereas larger grains (200–400 nm) also present in the samples are less effective. For the first time trapping and stabilization of NO_2 molecules in transition aluminas formed by a sol–gel route was shown.

Keywords: Grain size; Sol–gel processes; Electron microscopy; X-ray methods; Al_2O_3

1. Introduction

The influence of seeding or doping on the process of corundum formation beginning with alumina sols/gels via xerogels (containing boehmite or pseudoboehmite as the main components) and so-called transition aluminas has been studied using various methods during the past decades, e.g., X-ray diffraction,[1] thermal analysis (TG-DTA),[2,3] calorimetric[4] or dilatometric[5] measurements,^{27}Al NMR[6].

Baca et al.[7] have described the transformation of boehmite into α-alumina as a topotactic sequence, which forms several increasingly ordered transition aluminas. The final transition to α-alumina is a nucleation and growth type of reaction and the nucleation sites are usually oxygen vacancies and/or dislocations.[4] The temperature of the phase transition to corundum can be lowered by adding α-Al_2O_3 grains as seeds[1,8] and Fe^{3+} ions, accordingly. Corundum seeds enable an epitaxial growth of the corundum phase.

Aspects of the influence of seeding on corundum transformation (either lowering the temperature of phase transformation or enhancing corundum yields after heat treatment at a given temperature) have been discussed in the literature before.[9]

There are various mechanisms under discussion for explaining the action of Fe^{3+} ions and compounds in the process of corundum formation. Yarbrough and Roy[10] found that epitaxial growth of the corundum phase on dispersed α-Fe_2O_3 seeds results in a microstructure equivalent to that of a corundum seeded gel, whereas the addition of an $FeCl_3$ solution only leads to a small increase in nucleation frequency. According to the work done by Baca et al.[7] doping with Fe^{3+} ions should lead to defects in the structure of transition aluminas. These defects could initiate nucleation of α-Al_2O_3, i.e., epitaxial growth on α-Fe_2O_3 does not occur. The possibility of an enhanced mobility of O^{2-} in the Fe^{3+}-doped samples was also used to explain the reduction in temperature of corundum formation.[11]

To investigate the transformations from boehmite or pseudoboehmite xerogels to corundum a special combination of methods is favoured in the present paper. This study includes differential thermal analysis (DTA), X-ray diffraction (XRD), transmission electron microscopy (TEM) and electron paramagnetic resonance (EPR). Thus, by combining the pieces of information obtained from these macroscopic and microscopic methods, it should be possible to derive

* Corresponding author.
E-mail address: marianne.nofz@bam.de (M. Nofz).

0955-2219/$ – see front matter © 2004 Elsevier Ltd. All rights reserved.
doi:10.1016/j.jeurceramsoc.2004.04.014

common features and differences to describe the phase transformation and related processes caused by heat treatment.

TG-DTA coupled with evolved gas analysis by mass spectroscopy (MS) allowed thermally induced processes to be indicated and the gases released to be identified, simultaneously. X-ray diffraction was used to detect and identify crystalline phases and their precursors in the samples. TEM in direct combination with electron diffraction and energy dispersive X-ray analysis (EDX) gave an image of the size and morphology of particles and also contributed to the identification of crystalline phases. EPR spectroscopy was used to obtain information about the crystalline as well as the amorphous alumina matrices via spin probes. Ions with ^{6}S state, Fe^{3+} and Mn^{2+}, were used. Fe^{3+} ions play a two-fold role here: On the one hand they take an active part in the thermally initiated processes, i.e., at least lower the temperature of corundum formation. On the other hand Fe^{3+} ions can sensitively monitor changes of the alumina matrix including the formation and perfection of the corundum lattice. In contrast, traces of Mn^{2+} ions present in the samples under study here will especially yield information on thermally induced changes of the xerogels leading to the formation of transition aluminas.

Although EPR is originally concerned with the local properties of matter, there is a *parallelism* of EPR findings (especially in systems where both chemical reactions and aggregation or de-aggregation processes of spin probes occur) and the results of macroscopic investigations. Thus, a specific contribution to understanding thermally induced processes in less ordered, multiphase materials is to be expected.

In the present paper it will be shown how the parallelism mentioned above can be established by EPR evidence for

- the incorporation and structural rearrangement of Fe^{3+} and Mn^{2+} ions in xerogels and of Fe^{3+} in corundum seeds,
- the appearance of paramagnetic intermediates such as NO_2 or X–NO (e.g., X = Fe^{2+}) when the gels are thermally treated,
- the diffusion of Fe^{3+} ions into transition aluminas at and above 600 °C,
- the aggregation and de-aggregation of Fe^{2+} and Fe^{3+} ions to form $\{FeO_x\}$ species as a function of thermal energy brought into a transforming matrix of transition aluminas.

The aspect of linking EPR findings with the results of DTA, XRD and TEM appears to be unique with respect to the results available in the literature regarding the field of corundum formation starting with a sol–gel process.

2. Experimental procedure

2.1. Materials

Sols were prepared by the Yoldas method[12,13] by hydrolysis of Aluminium(III)-sec-butoxide in water at 75 °C. HNO_3 was added to peptise the resulting colloidal boehmite/pseudoboehmite particles. Fe(III) doping of the sols was achieved by performing hydrolysis in the presence of ferric nitrate solutions. α-Al_2O_3 seeding was done by adding an appropriate suspension to the sols. The suspension was prepared from α-Al_2O_3 (Alcoa CT 3000 SG) by wet milling and was stabilised with nitric acid. Particle diameters in the corundum suspension used for seeding were checked by TEM and appeared to be in the range of 200–400 nm for one fraction of the particles. A second fraction of corundum seeds is clearly smaller; here the diameters are in the range of about 20 nm, sometimes below. The dispersant was evaporated by maintaining the sols at ∼90 °C. Then the solid residue was further dried for 4 h at 120 °C to obtain the xerogels studied here. Table 1 summarises the main characteristics of these samples.

Table 1
Description of samples under study

Sample	Doping and seeding levels (mol% Fe_2O_3/Al_2O_3 with respect to Al_2O_3 formed from boehmite)
Fe000	0
Fe004	0.04
Fe013	0.13
Fe026	0.26
Fe052	0.52
Fe104	1.04
S000	0
S050	0.5
S100	1.0
S200	2.0
S400	4.0

2.2. Methods

All samples were studied using combined TG-DTA–MS measurements in a TAG 24 thermobalance (Setaram, France) operating at up to 1300 °C and equipped with a mass spectrometer for analysing the evolved gases. Samples were heated at a rate of 5 °C/min under air/nitrogen flow. Selected samples (Fe000, Fe026, Fe104, S100) were heated to 600 and 1000 °C, respectively, in a thermobalance and then cooled to room temperature.

EPR spectra in the X-band were taken at room temperature with an ERS300 spectrometer (Zentrum für Wissenschaftlichen Gerätebau, Germany). For convenience the effective g factors $g' = h\nu/\beta B$ (h = Planck's constant, ν = microwave frequency, β = Bohr magneton, B = magnetic induction) will be used to represent and discuss the findings. Although for Fe^{3+} ions the g value is close to 2, in the X-band effective g values g' of up to 20 can result because of the fine structure.

XRD measurements were performed on a Seiffert FPM7 diffractometer (Freiberg, Germany) with Cu-K_α radiation. Phases were identified by comparison with the ICSD powder diffraction file.[14]

TEM investigations were carried out with a JEOL 4000FX analytical Transmission Electron Microscope. Imaging, electron diffraction and EDX were used as methods to determine the size, habit and crystallographic phase of the particles in the various samples. Xerogel and alumina powders were dispersed by ultrasonic treatment in alcohol. The dispersion was poured onto a carbon film located on a grid and slowly dried on air.

3. Results

3.1. Thermal analysis (TG-DTA)

Fig. 1 shows the DTA curve of sample Fe000 as well as the findings on the corresponding gaseous decomposition products detectable by mass spectroscopy. The results of thermal analysis for the other samples (Table 1) in the temperature region of up to 600 °C are similar. All of these samples yield the following thermal effects:

(i) Endothermic:

A = desorption of water from the xerogel. For some samples this peak is split into two superimposed broad ones (A_1, A_2).

B = release of weakly bonded water and nitrogen oxides, and oxidation of organic components to yield H_2O and CO_2. The simultaneous detection of nitric oxides as well as of H_2O and CO_2 leads to the conclusion that nitrate ions are involved in the oxidation of the organics in the xerogel.

C = combined effect of dehydration and further oxidation superimposed on the thermal effect caused by the formation of γ-alumina. This was reported to have appeared between 400 and 550 °C by other authors.[15]

N = decomposition of nitrates.

(ii) Exothermic:

X = crystallisation of a so far unidentified system. X-ray structural analysis of a sample heated up to the maximum of this peak, i.e., 220 °C, only revealed the pattern for pseudoboehmite.

T = transformation to corundum.

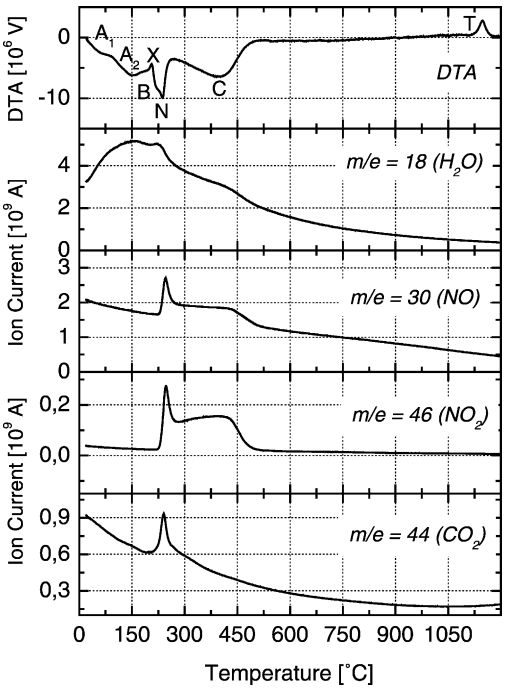

Fig. 1. DTA curve of sample Fe000 (5 °C/min; N_2/Air mixture) and evolved gases during TG-DTA experiment. Mass spectroscopic curves of molecules with relative masses *m/e* 18 (H_2O), 30 (NO), 46 (NO_2), and 44 (CO_2).

Gases resulting from the decomposition of the thermally non-stable components of the xerogels are completely released at about 600 °C.

Fig. 2 shows the exothermic peaks of corundum formation in the samples indicated together with the main parameters of the peaks. These are peak temperature T_p and peak area δA. Both, Fe^{3+} doping and Al_2O_3 seeding cause a similar thermal behaviour: the addition of rather small quantities of ferric iron ions or corundum particles causes the largest decrease in the temperature of corundum formation and the highest increase in peak area. This means that both additions enable the formation of corundum at a temperature far lower than 1100 °C. Otherwise this effect is limited, e.g., a further increase in the amount of dopants or seeds does not reduce the phase transformation temperature in a linear manner.

3.2. X-ray diffraction (XRD)

Fig. 3 shows the typical changes in the XRD patterns for a xerogel resulting from various heat treatments. Sample S100 serves as an example here. The X-ray diffraction patterns for all of the xerogels showed very broad reflections at the positions typical for boehmite (Fig. 3a). According to Bagwall and Messing[16] such broad reflections point to pseudoboehmite, i.e., a less ordered boehmite with a water content of 1.3–1.8 mol H_2O/1 mol Al_2O_3. Recently, Nguefack et al.[17] have provided a thorough discussion of the models for various boehmites. In the following, the term pseudoboehmite will be favoured to describe the precursors of γ-alumina studied here. After heating the sample to 600 °C (10 °C/min) the pseudoboehmite pattern vanished. Very broad reflections occurring between $2\theta = 15°$ and 40° and a more pronounced one at 45° indicate the presence of γ-alumina now (Fig. 3b). When the xerogel sample was heated to 1000 °C (10 °C/min), the pattern shown in Fig. 3c belonging to superimposed reflections of corundum as the main phase and of the residues of transition aluminas (see arrow) was obtained. Fig. 3d shows that after heating the sample to 1200 °C (5 °C/min) pure corundum with no further indication of the presence of transition aluminas was found.

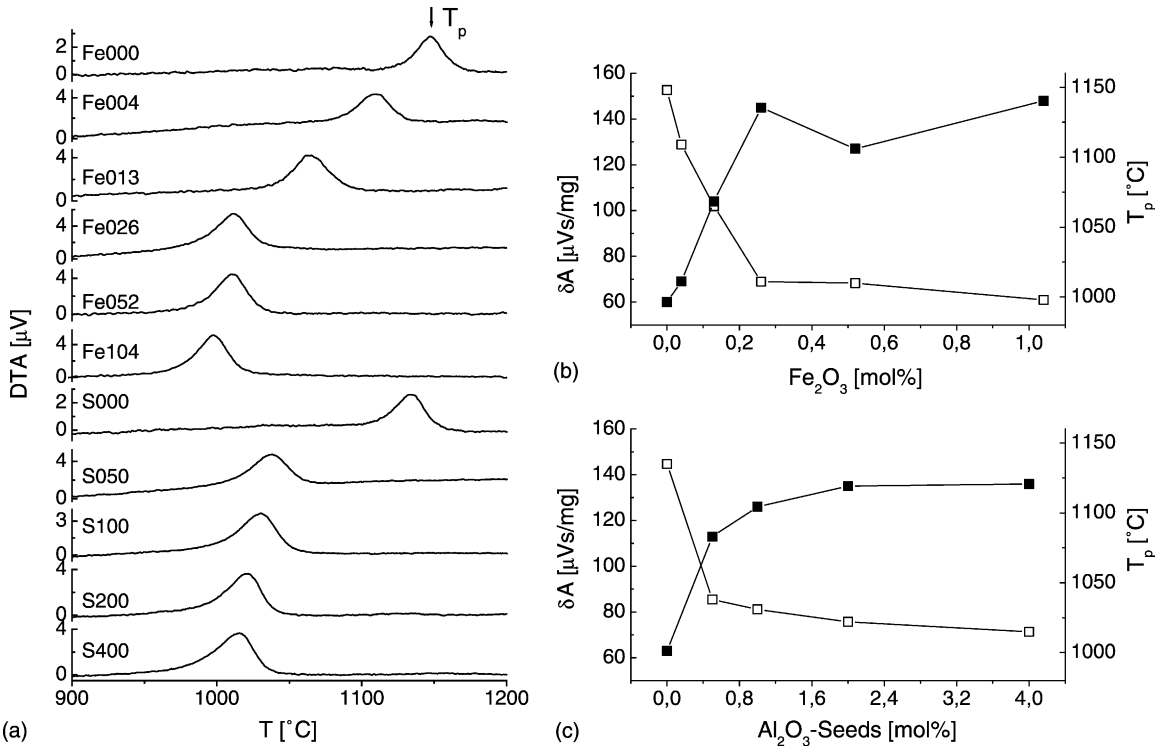

Fig. 2. DTA peaks of corundum formation of the samples indicated (a), their parameters: peak temperature (T_p: □), and peak area (δA: ■) as a function of Fe^{3+} (b), and corundum seed additions (c).

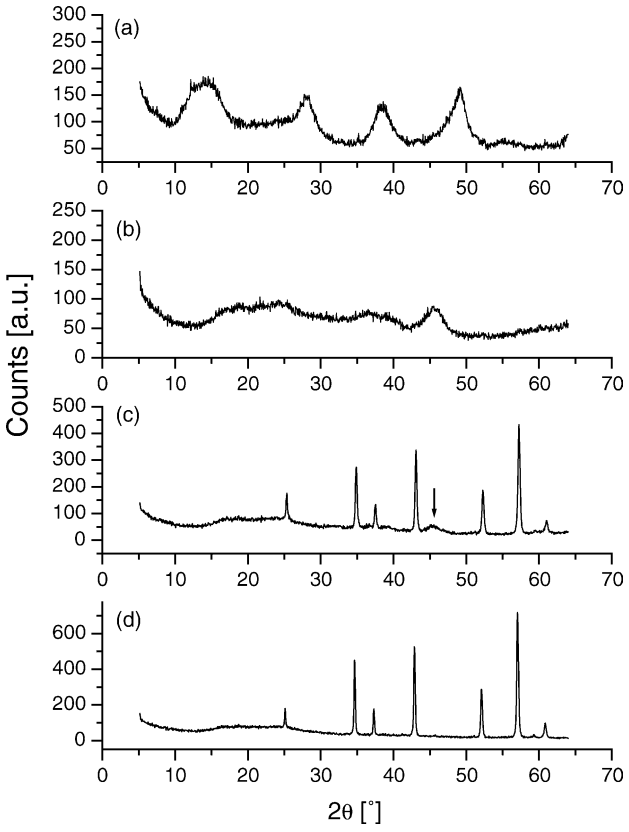

Fig. 3. X-ray diffraction patterns of sample S100 after different heat treatments: (a) 120 °C (xerogel), (b) heated up to 600 °C, (c) heated up to 1000 °C, and (d) heated up to 1200 °C.

3.3. Transmission electron microscopy (TEM)

TEM allows a more detailed investigation of individual particles. Fig. 4 gives examples of particle morphologies and crystalline phases found in xerogel powders. As shown in Fig. 4a and c collecting images of seeded and iron-doped samples, the xerogel matrices are formed by tiny particles (about 20 nm). These cannot be identified clearly, because their crystallinity is mostly weak and no single-crystal diffraction patterns could be obtained. The ring reflections of their polycrystalline diffraction patterns are broad due to the tiny dimensions. Thus, it is difficult to assign the majority of particles to a distinct crystal structure. Some pseudoboehmite was detected, based on XRD (see the preceding text), the respective *d*-values would also fit the analysis of electron diffraction here. The tiny pseudoboehmite particles are in close contact to the large corundum seeds (diameters of 100–400 nm), which are not single crystals, but show polycrystal reflections, cracks and rounded contours caused by milling processes (Fig. 4b). In the Fe^{3+}-doped xerogel boehmite/pseudoboehmite crystallites (Fig. 4c) and a needle shaped phase consisting mainly of iron and oxygen was detected (Fig. 4d).

After heating the xerogels to 600 °C almost all the water, nitrate and organic residues should be removed from the sample. Thus, in the seeded samples transition aluminas and corundum seeds should now be observable. As shown in Fig. 5a after that temperature treatment very small particles of transition aluminas result. According to

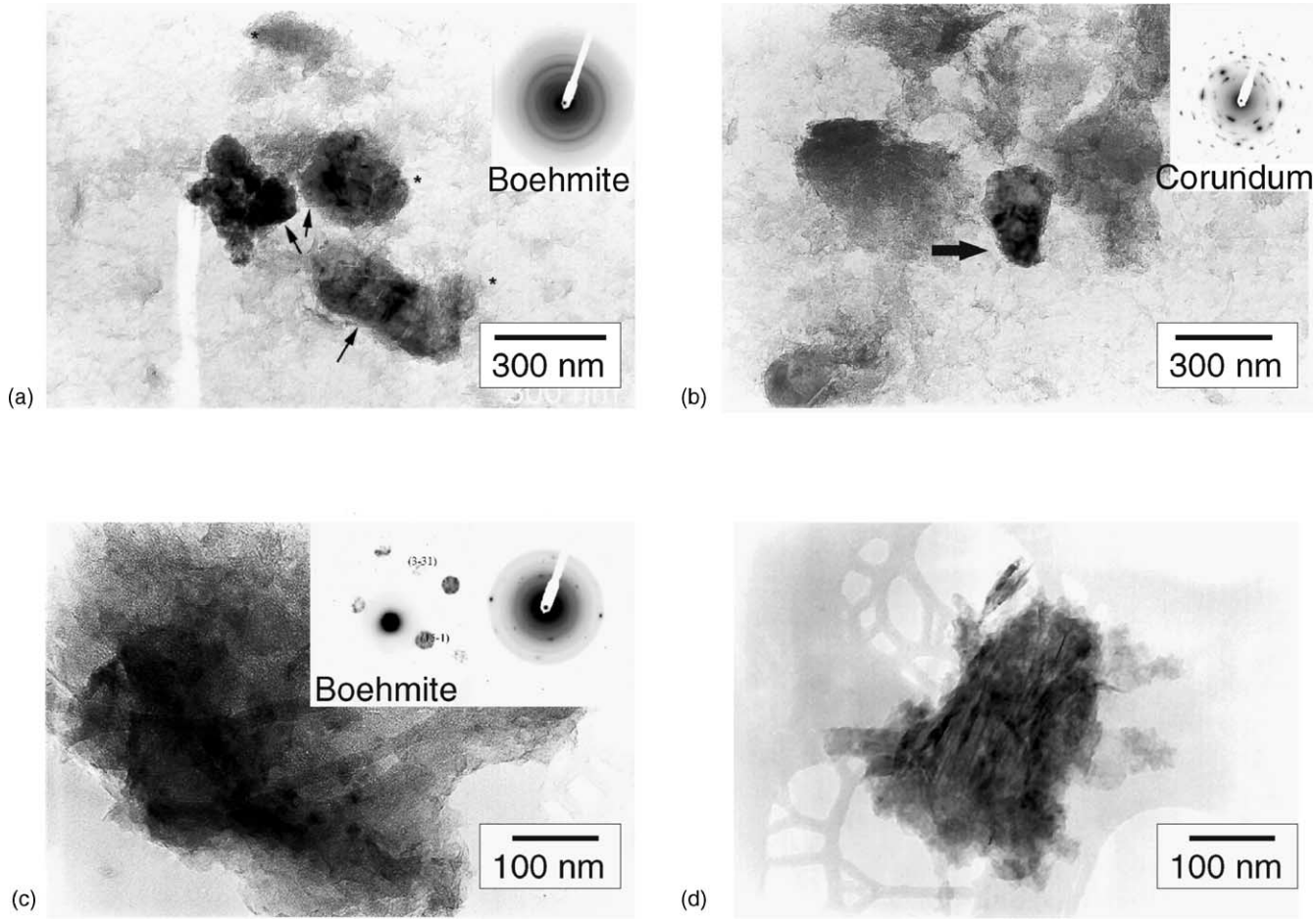

Fig. 4. TEM micrographs and electron diffraction patterns of xerogels. (a) Corundum seeds (arrows) surrounded by xerogel particles (stars), some cracks in the seeds can be seen. Polycrystal diffraction pattern of boehmite/pseudoboehmite, corresponding to the xerogel particles. (b) Polycrystalline corundum seed (arrow) and corresponding electron diffraction pattern, the seed is surrounded by xerogel particles. (c) TEM micrograph of xerogel particles of the highly with Fe ions-doped sample Fe104. Single-crystal diffraction pattern of a boehmite/pseudoboehmite particle (in $[1\,\bar{2}\,\bar{9}]$ orientation), aside polycrystalline diffraction pattern of agglomerates of the xerogel particles, referring to the presence of boehmite. (d) TEM micrograph of needles of the sample highly doped with Fe ions, these needles containing Fe and O mainly according to the EDX spectrograph (not shown). The electron diffraction patterns are ambiguous.

the electron diffraction investigations taken at several areas of the samples, some indication of γ- and δ-Al_2O_3 is obtained. It is of special interest, that in the areas of the tiny particles even α-Al_2O_3 could be identified by electron diffraction. This observation points to the presence of very small corundum seeds which could also be detected in the suspension, the smallest ones have diameters of less than 20 nm. Otherwise, the large seed particles, though still having some cracks, show single-crystal diffraction, i.e., defects originating from the milling process were to a certain extent removed ("healed over") by the heat treatment (Fig. 5b).

In contrast to the xerogel, particles of a discrete {Fe–O}-phase were not found in the iron-doped sample after the heat treatment at 600 °C (Fig. 5c). The xerogel has been transformed into a polycrystalline product. The appropriate polycrystalline reflections may be assigned to γ-Al_2O_3. They would also fit boehmite, which is however less probable taking into account the results from DTA analysis and XRD.

Keeping seeded and iron-doped samples at or above 1000 °C leads to the formation of corundum, according to the results of thermal analysis and X-ray diffraction. This is clearly demonstrated by the images and diffraction patterns in Fig. 6. In Fig. 6a it is possible to compare corundum seeds (~200 nm in diameter here) directly with the small corundum grains developed from the xerogel matrix. It is to be seen that corundum was also formed in the areas without close contact to the large corundum seeds. This again supports the assumption that the fraction of very small seeds was active here. In Fig. 6b a portion of a seeded sample is depicted. In the middle of the micrograph an area of "molten" appearing material is shown. According to the EDX investigations of this region aluminium and oxygen are the main constituents. This "molten" appearing region (identified by single-crystal diffraction patterns) is

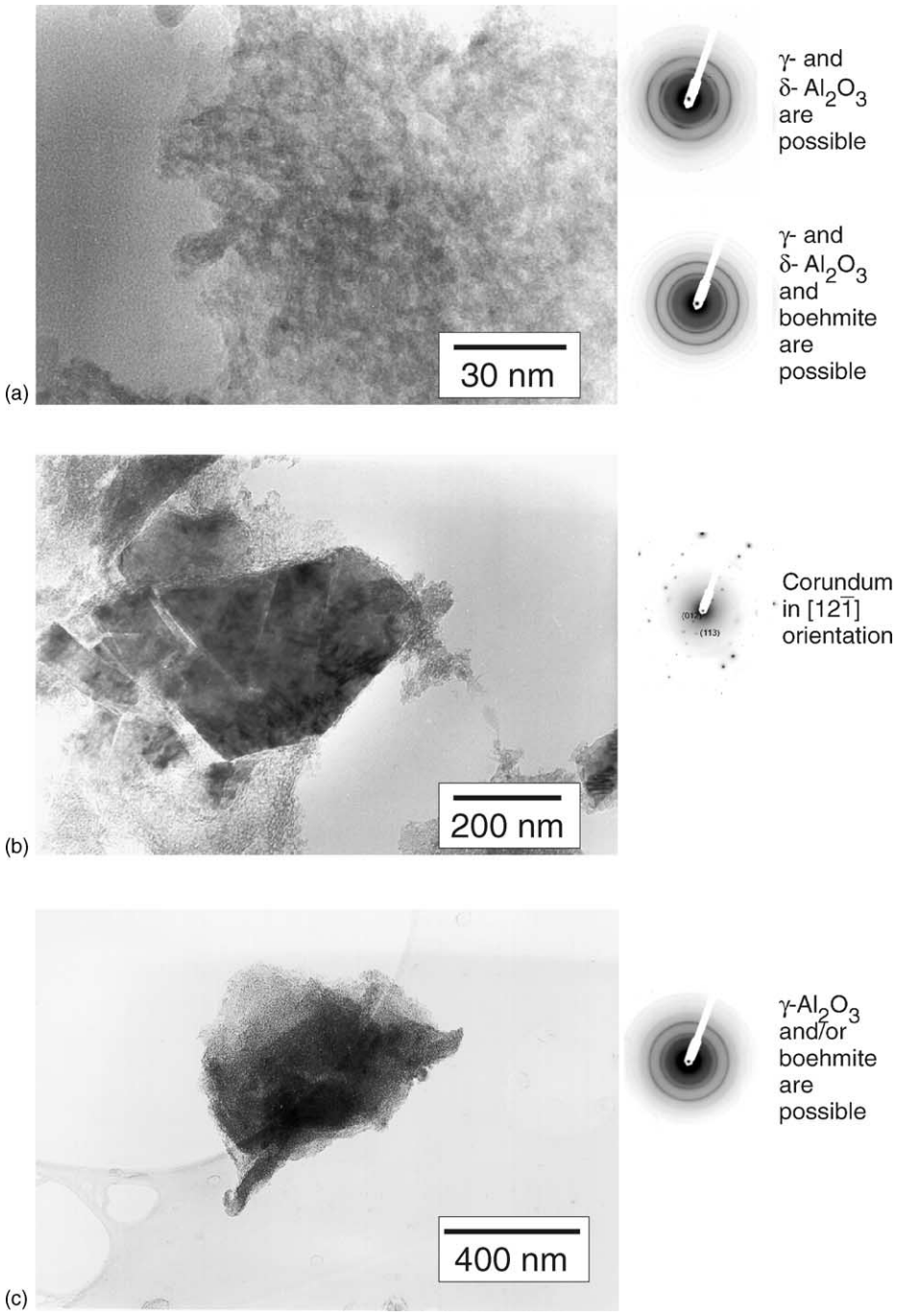

Fig. 5. TEM micrographs and electron diffraction patterns of xerogels after heat treatment at 600 °C. (a) Tiny particles in sample S100. The habit of the particles is not well defined, the respective polycrystal electron diffraction pattern shows a texture, caused by habit and/or orientation relationship of the particles, the presence of γ- and δ-Al_2O_3 could be detected. (b) Corundum seed with cracks (sample S100), after heating to 600 °C it shows single-crystalline regions (cp. diffraction pattern). The surrounding tiny particles are α- and δ-Al_2O_3 as well as boehmite/pseudoboehmite as identified in the polycrystal diffraction pattern. (c) Sample with high content of Fe-ions (Fe104), the particles are small with poor crystallinity, seen in the broad rings of diffraction pattern, that fits to γ-Al_2O_3 and boehmite/pseudoboehmite.

surrounded by tiny corundum crystals, identified through its polycrystalline reflections and its EDX spectrographs. The diffraction pattern in Fig. 6b shows both groups of reflections simultaneously.

Iron doping also succeeded in the formation of corundum at 1000 °C as can be seen from Fig. 6c. Spherical as well as needle-like corundum particles could be identified here. Furthermore, it is remarkable that now, again, needle shaped Fe–O particles are detectable (Fig. 6d). According to the diffraction patterns in combination with the ICPDS,[18] $Fe_{21,34}O_{32}$ or Fe_3O_4 ($FeFe_2O_4$) are possible phases here. The diffraction patterns contain areas of diffuse scattering

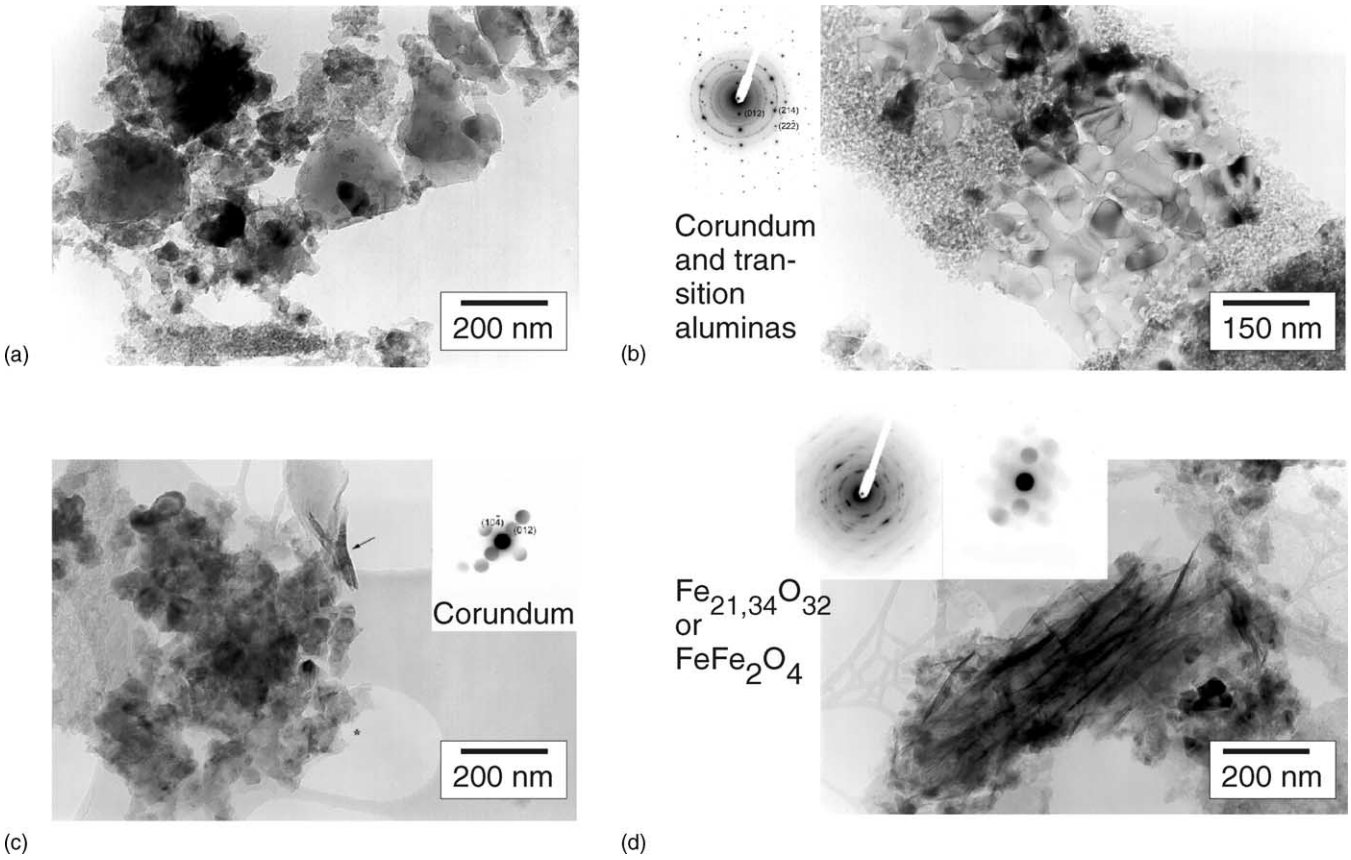

Fig. 6. TEM micrographs and electron diffraction patterns of xerogels after heat treatment at 1000 °C. (a) TEM micrograph of sample S100 with corundum seeds and tiny particles, identified as corundum and transition aluminas simultaneously present. (b) Between agglomerates of the small particles in sample S100 are "molten" appearing regions, identified as corundum. The diffraction pattern shows single-crystal reflections of an array of the "molten" appearing part (corundum in $[\bar{3}\,2\,\bar{1}]$ orientation) and polycrystalline ring reflections of the fraction of the small particles (transition aluminas) simultaneously. The polycrystalline diffraction fits to γ-, δ- and θ-Al_2O_3. (c) In the TEM micrograph of sample Fe104 different particle morphologies are to be seen: needle-like particle (arrow) and spherical ones (star). The single-crystal diffraction pattern of such a spherical particle is in accordance to corundum (in $[\bar{4}\,2\,\bar{1}]$ orientation). (d) Needle-like particles in sample Fe104; both diffraction patterns fit to $Fe_{21.34}O_{32}$ and $FeFe_2O_4$ (among other phases containing P or Al) and show diffuse scattering beside the reflections.

which can be caused by ordered defects which exist, e.g., in $Fe_{21,34}O_{32}$ as ordered vacancies.[19] Since these needles are not surrounded by corundum particles they could not have acted as seeds. Vice versa, it is to be expected, that during corundum formation the separation of an $\{FeO_x\}$ phase is forced by the limited ability of the corundum lattice to incorporate Fe^{3+} ions as point defects. Possibly also (intermediate) formation of Fe^{2+} plays a role here.

For comparison, the results of temperature treatment at 1000 °C on a nominally undoped and unseeded xerogel were also studied (Fig. 7). A peak temperature of corundum formation of 1148 °C was obtained. Thus, it is to be expected that the sample mainly consists of transition aluminas. Using TEM, aggregates of the very small, non-spherical particles are observable (Fig. 7). The poly-crystal electron diffraction patterns show a slight texture, caused by the shape and/or orientation relationship of these small particles. The patterns show the presence of γ-alumina as the main "phase", δ-alumina may also be a constituent of this product but the θ-phase is less probable.

3.4. Electron paramagnetic resonance spectroscopy (EPR)

X-band EPR spectra of the xerogels formed after drying at 120 °C show two characteristic resonances at $g' \sim 4.3$ and in the $g' = 2$ region, respectively (Figs. 8 and 9). Traces of Fe^{3+} are ubiquitously present in alumina compounds, if no specific purification treatments are performed. Thus, in the nominally undoped samples, Fe000 and S100, traces of Fe^{3+} ions can also be found. The asymmetric resonance at $g' \sim 4.3$ is typical for Fe^{3+} ions in a distorted rhombic co-ordination sphere.[20]

There is a six-line resonance at $g' \sim 2$ with a hyperfine splitting of ~9 mT taken directly from the experimental spectra. This can be assigned to Mn^{2+}. Nitric acid was identified as the source of these Mn^{2+} traces. The acid was added to peptise the sols and to stabilize the corundum suspension. This means that adding a corundum suspension to a sol will enhance the total amount of Mn^{2+} in the sample, and the ratio of Fe^{3+} to Mn^{2+} will be changed. This is

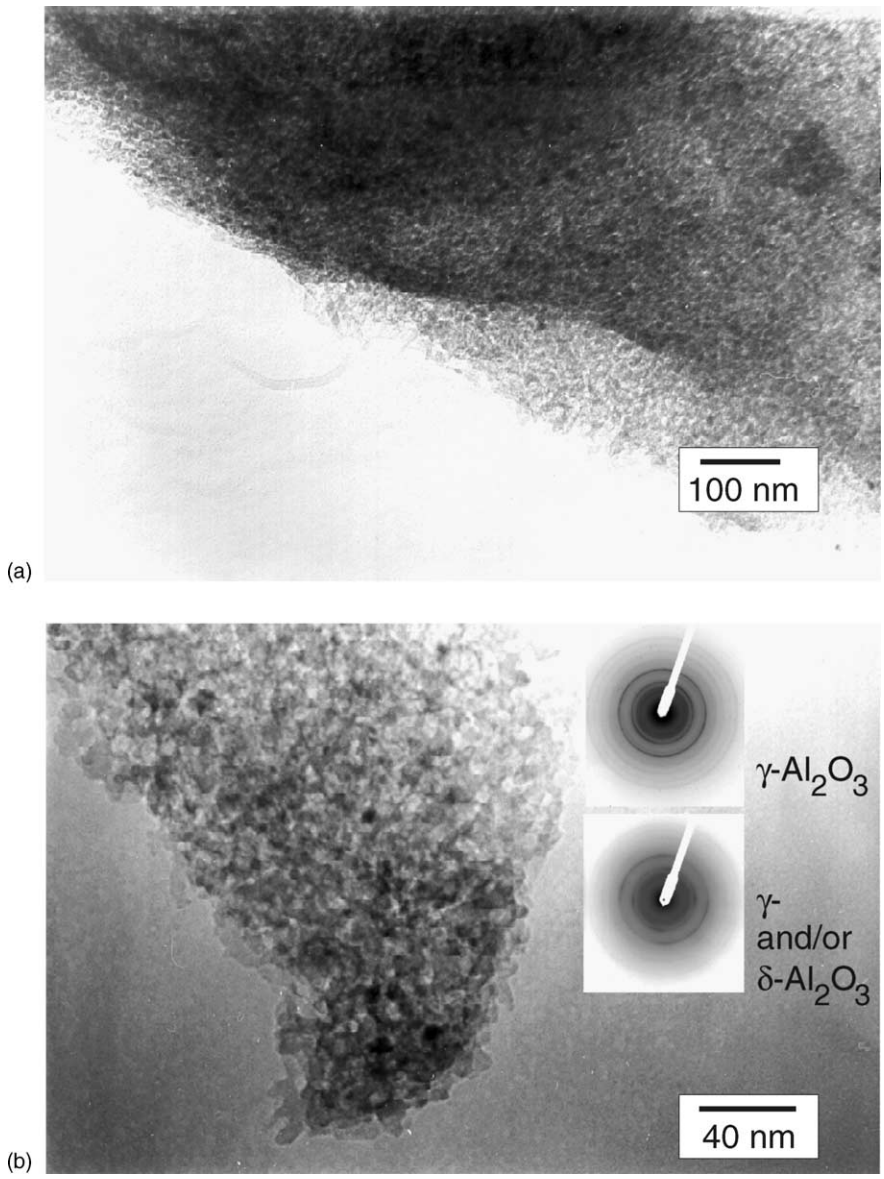

Fig. 7. TEM micrographs and electron diffraction patterns of xerogel Fe000 after heat treatment at 1000 °C. The particle dimensions are about 20 nm, their habit is not well defined, but longish structures are to be seen. Only polycrystalline diffraction patterns could be achieved, they are ambiguous and fit often to γ- and rarely to δ-Al_2O_3.

clearly indicated in Fig. 8 (compare parts a and e). As shown in Fig. 9, the ratios of the amplitudes of the resonances at $g' \sim 2$ and 4.3 are also altered after doping with Fe^{3+}. Doping with Fe^{3+} enhances the resonance at $g' \sim 4.3$ as expected (compare Fig. 9a and e).

Heating of the samples in steps causes characteristic changes of the spectra. After heating to 600 °C samples Fe000 and S100 show two effects:

(i) A triplet is observable superimposed on the Mn^{2+} sextet. This resonance can be assigned to trapped NO_2 molecules.[21] The hyperfine splitting constant results in $A = 5.35$ mT. To our knowledge, this is the first work which gives an indication of NO_2 molecules trapped in transition aluminas formed via a sol–gel process. It should also be mentioned here, that γ-irradiation of potassium nitrate at 300 °C did not lead to the formation of any detectable amounts of trapped NO_2 molecules.

(ii) The ratio in the amplitudes of Fe^{3+} and Mn^{2+} ions has been drastically changed. The amplitude of the Fe^{3+} resonance has increased, while that of the Mn^{2+} has decreased. These changes can be explained by oxidation processes. Oxidation of the ESR active Mn^{2+} ions and formation of inactive antiferromagnetically coupled Mn^{4+} species leads to a decrease of the amplitude of the Mn^{2+} sextet. Otherwise, oxidation of Fe^{2+} (which does not cause ESR signals at the temperatures used here) results in Fe^{3+} and thus in an increase of the

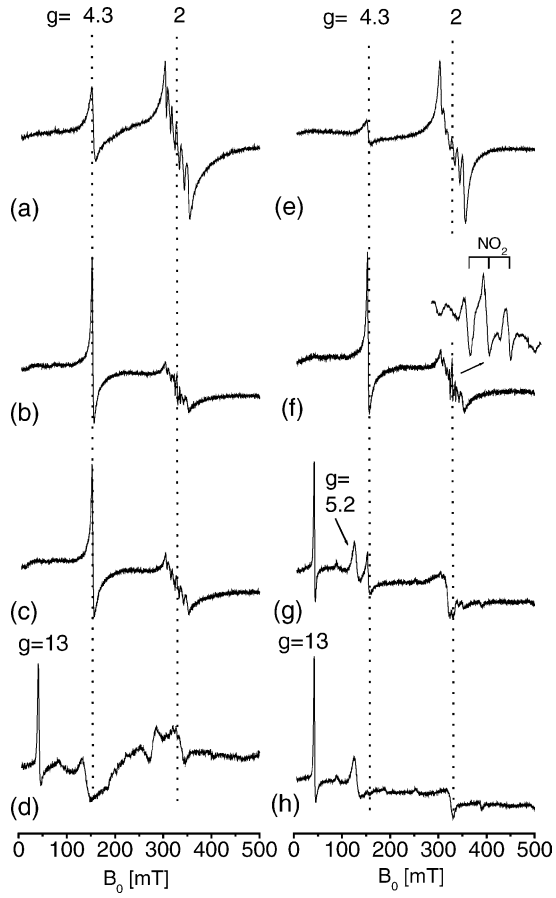

Fig. 8. EPR spectra (calibration of the *y*-axis is in arbitrary units) of samples Fe000 (a–d) and S100 (e–h). (a, e) Xerogels dried at 120 °C; (b, f) samples after heating up to 600 °C; (c, g) samples after heating up to 1000 °C; (d, h) samples after DTA experiment.

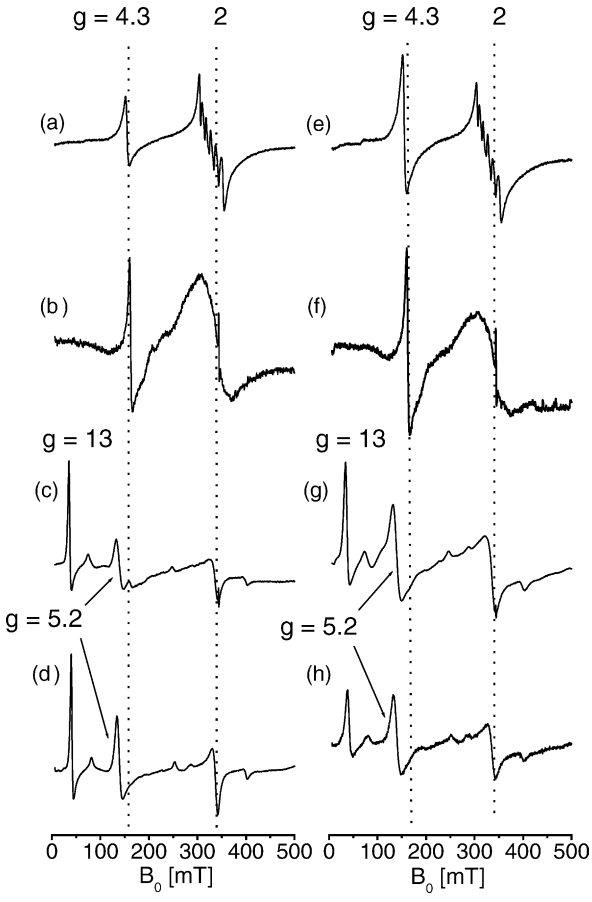

Fig. 9. EPR spectra (calibration of the *y*-axis is in arbitrary units) of samples Fe026 (a–d) and Fe104 (e–h). (a, e) Xerogels dried at 120 °C; (b, f) samples after heating up to 600 °C; (c, g) samples after heating up to 1000 °C; (d, h) samples after DTA experiment.

amplitude of the corresponding ESR resonance. Additionally, the effect of changes of the peak-to-peak linewidths of the ESR resonances from 8 mT (Fig. 8a) to 4 mT (Fig. 8b) has to be taken into account. As could be shown by spectra simulations[20,22] Fe^{3+} resonances at $g' \sim 4.3$ become narrower if the co-ordination polyhedra show stronger distortions. In the case of aluminas studied here, the transformation from pseudoboehmite (cf. Fig. 3a) to transition alumina (cf. Fig. 3b) should lead to a higher distortion of the alumina matrix and thus also of the Fe–O-polyhedra.

EPR spectra of Fe^{3+}-doped samples (Fe026 and Fe104 in Fig. 9) heated to 600 °C show remarkable differences compared to those of Fe000 and S100 described in the preceding text:

(i) Although thermal analysis showed that NO_2/NO was evolved from all samples in a similar way, there was no indication of NO_2 trapping (Fig. 9b and f). This discrepancy can be explained by magnetic interactions between paramagnetic NO_2 molecules and Fe^{2+}/Fe^{3+} which cause a broadening of the NO_2 triplet.

(ii) The Mn^{2+} sextet can no longer be detected possibly due to redox and aggregation processes of manganese species.

(iii) In the region at around $g' \sim 2$ a very broad resonance appears. This results from the magnetic interaction of iron ions, forming $\{FeO_x\}$-clusters. The latter ones point to the interaction of magnetically coupled iron ions bridged by oxygen atoms.

After heating to 1000 °C only slight changes occur in the spectra of sample Fe000 (Fig. 8c). According to DTA and XRD results, this sample should still be primarily composed of transition aluminas. Thus again, the resonances of Fe^{3+} at $g' \sim 4.2$ and of the Mn^{2+} sextet were observed. The NO_2 species are no longer detectable.

There are only very weak residues of the Mn^{2+} resonance remaining in the spectrum of the seeded sample (Fig. 8g). The asymmetric resonance at $g' \sim 4.3$ due to Fe^{3+} has become smaller and resonances at $g' \sim 13$, 5.6 and 2 have now become characteristic. This triple of EPR signals is an

X-band fingerprint of Fe^{3+} incorporated into corundum[22–24] (see also Fig. 9a and f). This means that Fe^{3+} ions are present in the remaining transition aluminas and in corundum, as well. For both Fe^{3+}-doped samples (Fig. 9c and g) the EPR spectra are determined by the pattern of Fe^{3+} ions incorporated into corundum. Additionally, for sample Fe026 a small residue of resonance is still detectable at $g' \sim 4.3$. Thus, a comparison of the spectra of the samples heated to 1000 °C shows that the content of transition aluminas decreases in the order Fe000 > S100 > Fe026 > Fe104, and conversely, that the content of corundum increases in this sequence, as was also to be expected from the results of TG-DTA and XRD.

In all samples resulting from TG-DTA experiments ($T >$ 1200 °C) corundum should now be the main phase. EPR spectra of all these samples are determined by the pattern of Fe^{3+} ions incorporated into corundum and further paramagnetic species are not detectable. Differences in the line width result from magnetic interactions in the Fe^{3+}-doped samples.[22,25]

The high sensitivity of the Fe^{3+} EPR pattern to changes in the distorted corundum lattices also allows a characterisation of the α-Al_2O_3 seeds used here (Fig. 10). Their suspension was prepared by wet milling commercially available corundum (Alcoa CT 3000 SG). The corresponding EPR pattern shown in Fig. 10a indicates a partially distorted corundum lattice at Fe^{3+} sites. The spectrum can be simulated by using the parameters given in the caption of Fig. 10. As Buzare et al.[22] have demonstrated, annealing the original sample Alcoa CT 3000 SG results in a less distorted corundum powder. Wet milling of this Alcoa corundum charge, i.e., formation of a suspension of even smaller corundum grains, leads to a further remarkable distortion of the initial corundum lattice. Fig. 10b–f shows the EPR spectra of the solids obtained after drying at 150 °C for 2 h and after subsequent heat treatments. It can be seen that after the milling procedure the co-ordination sphere of the Fe^{3+} indicated by the pattern of EPR resonances is different from that observed for well ordered corundum samples. Only the resonance at $g' \sim 13$ is detectable after drying at 150 °C. Further heat treatments enable a reorganisation of the corundum lattice. A temperature of 1050 °C is needed to obtain a pattern with the typical resonances at $g' \sim 13$, 5, and 2. The ratios between the amplitudes at $g' \sim 13$ and 5 are variable and significantly depend on the state of order of the corundum lattice. This means the ratios of the amplitudes clearly indicate how regular the actual corundum matrix is. The basis for this statement could be provided by a series of corresponding simulations.[22,23] Simulation of the spectrum in Fig. 10f was also possible here. The comparison of parameters given in the caption to Fig. 10 shows that after heat treatment at 1050 °C the corundum lattice has a higher degree of order than that of the initial powder (Fig. 10a).

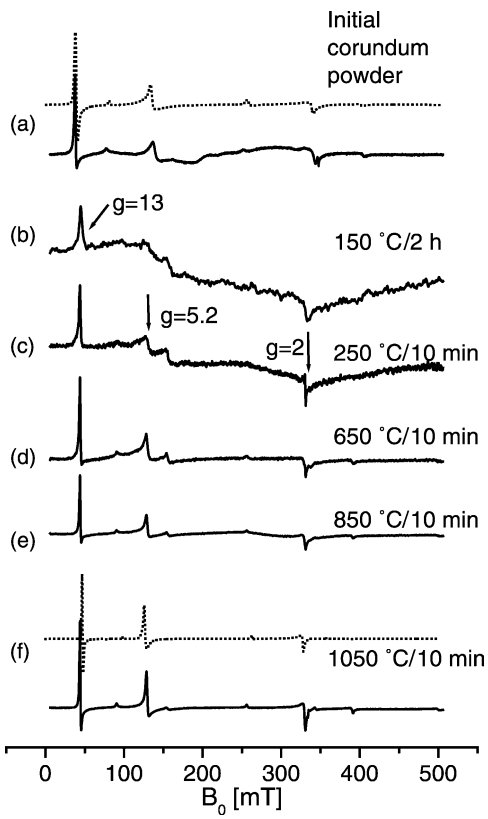

Fig. 10. EPR spectra (293 °C) of (a) the initial powder used for the preparation of a stable suspension of corundum seeds (solid line); (b) after drying the suspension at 150 °C for 2 h; and (c–f) after subsequent heat treatments for 10 min at the temperatures indicated. Dashed lines show spectra simulations using the following zfs parameters of Fe^{3+} ions in α-Al_2O_3 (reference 23): $b_2^0 = 1705 \times 10^{-4}\,cm^{-1}$, $b_4^0 = -108 \times 10^{-4}\,cm^{-1}$, $b_4^3 = 2181 \times 10^{-4}\,cm^{-1}$ and the distributions: (a) $\delta b_2^2 = 140 \times 10^{-4}\,cm^{-1}$, $\Gamma_0 = 3$ mT; (f) $\delta b_2^2 = 40 \times 10^{-4}\,cm^{-1}$, $\Gamma_0 = 1.5$ mT.

4. Discussion

Utilization of thermal analysis and XRD showed that there are three important temperatures for heat treatments: (i) 120 °C, the temperature for drying wet gels to prepare xerogels, i.e., a preparation of pseudoboehmite mixed with minor components such as nitrates, adsorbed water and organic residues from the sec-butanol; (ii) 600 °C, the temperature at which a majority of volatile components is evolved and gamma-alumina has formed; (iii) 1000 °C, the temperature at which corundum should have formed in seeded and Fe^{3+}-doped samples, whereas in undoped samples such as Fe000 the transition aluminas are still present. For this reason, samples in the TEM, XRD and EPR studies were heated to these temperatures.

4.1. Characterization of the xerogel matrix

As expected, pseudoboehmite was obtained as the typical product of the hydrolysis of Al-alkoxides in acidic media at temperatures above 75 °C. This means, doping with Fe^{3+} or seeding with a corundum suspension does not significantly change the type of alumina which forms the xerogel matrix.

As a consequence, during thermal treatment the sequence of phase transformations is maintained for Fe^{3+}-doped and seeded pseudoboehmites, respectively. According to Bye and Simpkin,[11] Fe^{3+} has no significant influence on the type of transition aluminas formed. δ-Al_2O_3 was the main intermediate phase produced from both pure γ-Al_2O_3 and that containing Fe^{3+} in solid solution—although the addition of Fe^{3+} greatly reduced crystallinity in the δ-phase.

These new findings result from the TEM and EPR studies of the xerogels presented here:

(a) Doping with Fe^{3+} ions yields at least two different Fe^{3+} species in the xerogels: (i) Isolated Fe^{3+} ions incorporated into pseudoboehmite particles (sites exhibit rhombic distortion, as indicated by an EPR resonance at $g' \sim 4.3$); (ii) ferric (perhaps also ferrous) ions as part of a separate $\{FeO_x\}$ phase (broad EPR resonance at $g' \sim 2$). Explicit detection of $\{FeO_x\}$ in Fe^{3+}-doped samples using TEM showed a needle shaped species consisting mainly of iron and oxygen. The formation of $\{FeO_x\}$ indicates that under the conditions chosen (time, temperature), the pseudoboehmite is not able to incorporate all the Fe^{3+} offered.

(b) Another implication of adding Fe^{3+} (and simultaneously, also, NO_3^-) concerns the xerogel matrix. Some parts of the iron-doped sample Fe104 are not stable under the influence of the electron beam and thus could not be investigated; some parts exhibit a marginally higher crystallinity and a few a greater grain size than was observed in the seeded material. This can be seen in the narrowing of the polycrystalline reflections and in the appearance of spots in the rings, as depicted in Fig. 4c. Even single crystalline patterns of boehmite can be successfully observed, as can also be seen in that figure. This is in contrast to sample Fe026 which has a smaller amount of dopants, and where the crystallinity of the boehmite particles is very weak and the grain size very small.

(c) Two fractions of corundum particles (∼20 nm and 200–400 nm) were identified by TEM in the dried corundum suspension. The fraction of very small (∼20 nm) corundum particles from the corundum suspension could not be distinguished from the pseudo-boehmite matrix in seeded xerogels by diameter or habit but only by electron diffraction results. Seeds are embedded in a pseudo-boehmite matrix which is not different from the undoped and unseeded xerogel. Large corundum grains (200–400 nm) can easily be distinguished from a xerogel matrix and characterized using TEM.

(d) Mn^{2+} ions are incorporated into the pseudoboehmite matrix as non-aggregated centers.

4.2. Alumina obtained after heating xerogels to 600 °C

According to the results of thermal analysis (TG-DTA–MS), after heating the xerogels to 600 °C any water, organic compounds or nitrate should be removed and the transition aluminas, most probably γ-alumina, should have formed.

The X-ray diffraction patterns of the heat treated xerogels point to a weakly ordered product. A characteristic reflection at $2\theta = 45°$ indicates the presence of transition aluminas, γ- as well as δ-alumina fit this X-ray reflection. This was confirmed and specified by the results of the electron diffraction patterns (Fig. 5). Because of the tiny dimensions (as little as 10 nm) of the particles and their strong agglomeration, especially in the case of iron-doped samples, no single-crystal diffraction patterns could be achieved. According to the electron diffraction investigations, as a result of the regime of heat treatments of up to 600 °C in the samples doped with iron ions pseudoboehmite has transformed into γ-alumina (other transition aluminas were not included in the data treatment for the Fe-doped samples). The seeded samples show γ- and δ-alumina as transformation products of the pseudoboehmite. Any amount of α-alumina which could be detected in the seeded sample probably results from the tiny alumina grains originally created by the preliminary milling process.

The following new aspects with respect to heat treatments of up to 600 °C will especially be emphasized here:

- The detection of the intermediates NO and NO_2 shows the ability of transition aluminas to stabilize and trap these reactive molecules.
- The consumption of $\{FeO_x\}$ present in the xerogel by diffusion of Fe^{3+} into the matrix of transition aluminas: In the Fe^{3+}-doped sample particles of a separate $\{FeO_x\}$ phase (as observed before in the xerogel) could not be detected. This might be due to the fact, that TEM is always able to investigate only a very small part of the sample. Otherwise, it is more probable that the transition aluminas when heated to 600 °C are able to incorporate a certain amount of Fe^{3+} ions. This conclusion is assisted by some EDX spectrographs of the small particles which show little iron content in the agglomerates of the transition alumina particles and by EPR findings. In a separate experiment a mixture of xerogel with ferric nitrate was kept at 850 °C. It could be shown by using the line widths and intensities of the Fe^{3+} resonance at $g' \sim 4.3$ as a qualitative measure, that Fe^{3+} diffused into transition aluminas. This ability to incorporate Fe^{3+} ions into transition aluminas would also explain the observations previously described in the literature.[4] On the one hand, increased amounts of Fe^{3+} ions offer a good precondition for the formation of oxygen vacancies and dislocations. Thus the idea is supported, that formation of an α-Fe_2O_3 phase is not essential to enhance the velocity or to decrease the temperature of corundum formation in iron-doped samples. On the other hand, the capacity of transition aluminas to incorporate isolated Fe^{3+} ions is limited and depends on temperature. If a certain concentration of Fe^{3+} is present in the transition aluminas, then a further supply of ferric iron ions will lead to the formation of very small $\{FeO_x\}$

aggregates and finely dispersed crystallites of α-Fe_2O_3. It is known[11], that hexagonal α-Fe_2O_3 is formed from the cubic γ-phase at ∼350 °C. The small, finely dispersed crystallites of α-Fe_2O_3 can serve as nuclei for corundum formation as has already been discussed in the literature.[10]

- Corundum seeds distributed in the matrix are mainly "healed over" with respect to macroscopic defects. Thus, even small corundum particles could be detected by utilization of the electron diffraction ring patterns in the sample region with only small particles (see Fig. 5a). A comparison of the milled corundum seeds before and after tempering shows clear differences in the crystal quality. After the milling process, we observed a fraction of hackled corundum grains with diameters of between 20 and 40 nm, some of them even smaller; the latter most show polycrystalline electron diffraction patterns. A second fraction of corundum seeds was larger and had diameters of between 200 and 400 nm. These seeds often showed cracks and evidence of plastic deformation, their crystalline structure was disturbed and only polycrystal diffraction could be achieved. After tempering, the fraction of large corundum seeds is healed over, some cracks are still to be seen, but electron diffraction investigations show single-crystal patterns.
- In the transition aluminas formed from Fe000 and seeded samples, respectively, Mn^{2+} remains detectable, but in the iron-doped samples the Mn^{2+} sextet is not observable. There may be two reasons for this: (i) Mn^{2+} takes part in redox reactions with Fe^{2+}/Fe^{3+}, (ii) Mn^{2+} interacts with $\{FeO_x\}$-clusters.

4.3. Alumina obtained after heating the xerogels to 1000 °C

Finally, corundum is formed during thermal treatment at and above 1000 °C. As observed by other authors earlier,[1,4,8] the addition of seeds or of Fe^{3+} ions results in a decrease in the temperature of phase transformation to corundum. This effect is not linear with respect to the seeds or dopants added, as confirmed in this work.

In sample Fe000, according to the DTA measurements, corundum formation should start at temperatures above 1100 °C, thus formation of corundum should not be expected here. In contrast, in Fe^{3+}-doped (Fe026, Fe104) and corundum-seeded (S100) samples the phase transition to corundum could start at temperatures of around 1000 °C.

In undoped, unseeded sample mainly transition aluminas are present as expected, but traces of α-alumina have also formed. The transformation of the undoped sample does not proceed to a single definite phase; we found γ- as well as δ-Al_2O_3, but with smaller amounts of the latter (TEM).

In Fe^{3+}-doped and corundum-seeded samples large percentages of the samples have transformed to corundum, but residues of transition aluminas are still present according to the results of XRD and EPR.

The regime up to 1000 °C delivers the complete transformation to corundum in a sample weakly doped with Fe^{3+} ions; no other phases and no other elements than Al or O could be detected by TEM.

The sample with the higher iron content has also transformed to corundum, there are small amounts of impurities and a portion of $\{FeO_x\}$ phases which fit either $Fe_{21.34}O_{32}$ or γ-Fe_2O_3 (tetragonal Maghemite). It follows, that at this temperature the corundum lattice is not able to incorporate larger amounts of Fe^{3+}; thus an additional $\{FeO_x\}$ phase must have been formed after heating the sample to 1000 °C.

In the seeded sample tempered to 1000 °C, a series of Al_2O_3-phases (γ-, δ-, θ-, α-) could be detected by TEM imaging in combination with electron diffraction as transformation products of the xerogel. "Molten" appearing areas were found in the seeded sample. According to EDX results, impurities are not responsible for this unexpected morphology.

In seeded xerogels the transformation to corundum is preferred in those parts of the samples which are close to small corundum seeds, larger ones are less effective.

After transformation to corundum Mn^{2+} ions are no longer detectable by EPR.

5. Conclusions

The main issue of this work was to have a combined spectroscopic and macroscopic characterisation of the actions of Fe^{3+} ions and corundum seeds, respectively, during thermally induced transformations of boehmite or pseudoboehmite xerogels. Therefore it was important, firstly, to identify the main constituents of the xerogels under discussion here. Under the conditions chosen here for sol syntheses, the xerogels should be composed of boehmite or pseudoboehmite as the main phase (compare, e.g., Ngueack et al.[17] and Pierre and Uhlmann[26]), (basic) aluminium nitrate and volatile components such as adsorbed water and sec-butanol.

Looking at the results of thermal analysis in combination with MS and XRD, it was shown that on heating to 1200 °C the pseudoboehmite xerogel releases water, nitric oxides and residues of organic compounds while transforming to corundum via transition aluminas.

From the view of materials science, especially concerning the mechanisms of doping with Fe^{3+} ions and seeding with corundum grains, the following conclusions can be drawn concerning thermally induced transformations at temperatures of up to 1200 °C:

- Heating Fe^{3+}-doped pseudoboehmite xerogels causes dissolution, as well as crystallization of $\{FeO_x\}$ phases. Their formation and stability is governed by the state of the alumina matrix. In the result, various Fe^{3+} species can exist. Large $\{FeO_x\}$ particles detected in xerogels by TEM do not act as nucleation sites.

- Perfection of the corundum grains used as seeds has not previously been taken into account. Here a combined microscopic (TEM) and spectroscopic (EPR) view could be taken. It was shown, that after heat treatments at 600 °C the macroscopic defects from the milling process are nearly "healed over" and that after heat treatments at 650 °C rearrangement of the corundum lattice was indicated by the Fe^{3+} EPR pattern.
- Grain sizes for the seeding corundum particles were not uniform in the samples studied here. Small (about 20 nm) particles are the more active nucleation sites compared to large ones (200–400 nm).

The following specific contributions of EPR spectroscopy can be summarized:

- Structural changes of and transitions between aluminas are well and sensitively reflected by the EPR spectra of Fe^{3+} and Mn^{2+} ions as well as by trapped NO_2.
- Spectroscopic, structural and chemically relevant information was obtained about several kinds of Fe^{3+} species and their incorporation into amorphous and crystalline alumina phases. A sensitive indication of the local formation of corundum nanocrystallites was possible, allowing an insight into the local rearrangements which begin before the process of phase formation proceeds.
- Isolated Mn^{2+} ions are only observable in xerogels and transition aluminas, i.e., in highly disordered regions of the samples.
- The detection of NO_2 molecules trapped in sol–gel derived transition aluminas was achieved for the first time.
- On heat treatment of freshly prepared corundum seeds, not only cracks and rounded contours are "healed over". A structural reconstruction of the lattice was also initiated.

Acknowledgements

We wish to thank R. Sojref for preparing the stable corundum suspensions and A. Zehl for technical assistance at the EPR measurements. The project was financially supported by the Deutsche Forschungsgemeinschaft.

References

1. Urretavizcaya, G. and Porto Lopez, J. J., Thermal transformation of sol–gel alumina into α-phase. Effect of α-Al_2O_3 seeding. *Mater. Res. Bull.* 1992, **27**, 375–385.
2. Chen, Y.-C., Huang, C.-Z., Al, X. and Wang, B.-Y., Formation and bonding mechanism of solution derived α-Al_2O_3 coating on carbide substrate. *Surface Eng.* 2001, **17**(4), 279–285.
3. Frost, R. L., Kloprogge, J., Russell, S. C. and Szetu, J. L., Dehydroxylation and structure of alumina gels prepared from trisecbutoxyaluminium. *Thermochim. Acta* 1999, **329**, 47–56.
4. Kumar, K.-N. P., Tranto, J., Kumar, J. and Engell, J. E., Pore-structure stability and phase transformation in pure and M-doped (M = La, Ce, Nd, Gd, Cu, Fe) alumina membranes and catalyst supports. *J. Mater. Sci. Lett.* 1996, **15**, 266–270.
5. Vendange, V. and Colomban, Ph., Densification mechanisms of alumina, aluminosilicate and aluminoborosilicate gels, glasses and ceramics. *J. Sol–gel Sci. Technol.* 1994, **2**, 407–411.
6. Colomban, Ph. and Vendange, V., Sintering of alumina and mullites prepared by slow hydrolysis of alkoxides: the role of the protonic species and pore topology. *J. Non-Cryst. Solids* 1992, **147/148**, 245–250.
7. Baca, L., Plewa, J., Pach, L. and Opfermann, J., Kinetic analysis of crystallization of α-Al_2O_3 by dynamic DTA technique. *J. Therm. Anal. Calorimetry* 2001, **66**, 803–813.
8. Messing, G. L. and Kumagai, M., Low-temperature sintering of α-alumina-seeded boehmite gels. *Am. Ceram. Soc. Bull.* 1994, **73**(10), 88–91.
9. Nordahl, C. S. and Messing, G. L., Thermal analysis of phase transformation kinetics in α-Al_2O_3 seeded boehmite and γ-Al_2O_3. *Thermochim. Acta* 1998, **318**, 187–199.
10. Yarbrough, W. A. and Roy, R., Microstructural evolution in sintering of AlOOH gels. *J. Mater. Res.* 1987, **2**(4), 494–515.
11. Bye, G. C. and Simpkin, G. T., Influence of Cr and Fe on Formation of α-Al_2O_3 from γ-Al_2O_3. *J. Am. Ceram. Soc.* 1974, **57**(8), 367–371.
12. Yoldas, B. E., Alumina sol preparation from alkoxides. *Am. Ceram. Soc. Bull.* 1975, **54**, 286–290.
13. Yoldas, B. E., Alumina gels that form porous transparent Al_2O_3. *J. Mater. Sci.* 1975, **10**, 856–860.
14. Powder Diffraction File, ICPDS-ICDD2001.
15. Schimanski, J., Production of dispersible aluminas and their use in different applications. *Key Eng. Mater.* 1998, **150**, 161–170.
16. Bagwall, R. B. and Messing, G. L., Critical factors in the production of sol–gel derived porous alumina. *Key Eng. Mater.* 1996, **115**, 45–64.
17. Nguefack, M., Popa, A. F., Rossignol, S. and Kappenstein, C. h., Preparation of alumina through a sol–gel process. Synthesis, characterization, thermal evolution and model of intermediate boehmite. *Phys. Chem. Chem. Phys.* 2003, **5**, 4279–4289.
18. Powder Diffraction File, ICPDS-ICDD2002.
19. Shmakov, A. N., Kryukova, G. N., Tsybulya, S. V., Chuvilin, A. L. and Solovyeva, L. P., Vacancy ordering in γ-Fe_2O_3: synchrotron X-ray powder diffraction and high-resolution electron microscopy studies. *J. Appl. Cryst.* 1995, **28**, 141–145.
20. Scholz, G., Stösser, R., Krossner, M. and Klein, J., Modelling of multifrequency ESR-spectra of Fe^{3+} ions in crystalline and amorphous materials: a simplified approach to determine statistical distributions of spin-spin coupling parameters. *Appl. Magn. Res.* 2001, **21**, 105–123.
21. Weil, J. A., Bolton, J. R. and Wertz, J. E., *Electron Paramagnetic Resonance*. John Wiley & Sons, Inc., New York, Chichester, Brisbane, Toronto, Singapore, pp. 262–266.
22. Buzare, J. Y., Silly, G., Klein, J., Scholz, G., Stösser, R. and Nofz, M., Electron paramagnetic resonance investigations of α-Al_2O_3 powders doped with Fe^{3+} ions: experiments and simulations. *J. Phys.: Condens. Matter* 2002, **14**, 10331–10348.
23. Scholz, G., Stösser, R., Klein, J., Silly, G., Buzare, J. Y., Laligant, Y. *et al.*, Local structural orders in nanostructured Al_2O_3 prepared by high energy ball milling. *J. Phys.: Condens. Matter* 2002, **14**, 2101–2117.
24. Stösser, R. and Scholz, G., Fe^{3+} ions in amorphous solids: EPR on mechanically and chemically amorphized Al_2O_3. *Appl. Magn. Res.* 1998, **15**, 449–468.
25. De Biasi, R. S. and Rodriguez, D. C. S., Influence of iron concentration and particle size on the ESR line width of Al_2O_3:Fe^{3+} powders. *J. Mater. Sci. Lett.* 1983, **2**, 210–212.
26. Pierre, A. C. and Uhlmann, D. R., Amorphous aluminum hydroxide gels. *J. Non-Cryst. Solids* 1986, **82**, 271–276.